Accurate 3D Acquisition of Freely Moving Objects
Blais, François; Picard, Michel; Godin, Guy

National Research Council Canada   Conseil national de recherches Canada

Canada

National Research
Council Canada

Conseil national
de recherches Canada

Institute for
Information Technology

Institut de technologie
de l'information

NRC·CNRC

*Accurate 3D Acquisition of Freely Moving Objects **

Blais, F., Picard, M., Godin, G.
September 2004

Canada

Accurate 3D acquisition of freely moving objects

François Blais, Michel Picard, Guy Godin
National Research Council of Canada
Institute for Information Technology
Ottawa, Ontario, Canada, K1A 0R6
Email: Francois.Blais@nrc-cnrc.gc.ca

Abstract

This paper presents a new acquisition method for 3D laser scanners that combines imaging, fast geometrical object tracking, and automatic pose estimation to register range profiles of freely moving objects. The method was developed to solve the constraint of rigidity between free-moving objects and a 3D scanner while preserving the accuracy of the range measurements. Rigidity constraint imposes that a 3D scanner or any external positioning devices must be perfectly stable relative to the object during scanning. This is often impossible for moving structures such as when using scaffolding, industrial conveyers, or robotic arms. The method starts by creating a rough, partial, and distorted estimate of the model of the object from an initial subset of sparse range data. Then, it recursively improves and refines the model by adding new range information. In parallel, real-time tracking of the object is performed to center the scan on the object. A high-resolution and accurate 3D model of a free-floating object, and real-time tracking of its position is obtained.

Keywords: 3D range imaging, hand-held scanner, tracking, portable, registration, modeling.

1. Introduction

Constraining an object to be perfectly rigid and its position to be stable relative to a 3D scanner system is a major requirement that must be maintained during the acquisition of 3D range data. Constrained rigidity means that there are no relative motions or vibrations between the sensor system and the object (static mode) or that any motion can be accurately measured using external positioning devices such as optical or magnetic trackers, inertial guidance systems, translation or rotation stages (controlled motion). Current 3D acquisition systems impose that the object is perfectly stable and rigid relative to the scanner or at least to the motion detection device during the whole acquisition.

Table 1 shows typical acquisition times needed to acquire high-resolution 3D images assuming a 3D acquisition rate of 10 kHz. Mechanical stability must be guaranteed for more than 2 minutes for an image of 1024×1024 rigels (Range ImaGe ELements). Even 2 seconds for a much smaller 128×128 image can be problematic in many applications.

Table 1: Typical acquisition speed using 3D raster imaging.

Image Size		(sec)
128	128	1.6
256	256	6.6
512	512	26.2
1024	1024	104.9
Acquisition rate		10 kHz
Retrace time		2 ms

Stability is therefore paramount in acquiring high accuracy images and any mechanical oscillations or vibrations will seriously compromise the accuracy. Figures 1 to 3 are practical examples that illustrate the use of 3D range sensors, from the controlled lab environment to the more difficult field application. In the case of Figure 1, rigidity is provided by the mechanical infrastructures. With the portable system of Figure 2, the rigidity constraint between the object and the camera depends on the stability of the tripod, which will be hampered by the presence of vibrations from the ground. For example, people walking or nearby vehicles can induce angular oscillations in the ground and in the tripod far exceeding 1 mrad in amplitude that translates to more than 1 mm of error at a distance of 1 m from the camera. The use of scaffoldings as shown in Figure 3 is now very common; the problem of stability of the structure will amplify the errors by several orders of magnitude.

Positioning equipment such as optical trackers is only a partial solution; an absolute mechanical rigidity between the optical tracker and the object must still be

maintained. It assumes that the optical tracker must be perfectly mounted relative to the object under investigation, which is not allowed in many applications. Figure 4 is a 3D inspection application currently under investigation by Neptec, NASA, NRC, and the Canadian Space Agency for on-orbit inspection of the tiles of the Space Shuttle fleet following Discovery disaster. The 3D laser camera will be mounted on the tip of an extension boom to the Canada Arm. Mechanical models show that a residual oscillation of more than 5 cm at 0.7 Hz at the tip of the boom is expected.

Figure 1: Lab configuration, rigidity between the scanner and the object is obtained by the use of a stable mechanical infrastructure.

Figure 2: 3D laser scanner on a rigid tripod for field utilization. The quality of the tripod can provide relative stability. However, vibrations and oscillations induced by wind, people, or passing vehicles can seriously degrade the accuracy of the system.

Removing the constraints associated with rigidity will solve the problem of stability of Figures 2 and 3 and more important will dramatically reduce the costs associated with complex mechanical structures as in Figure 1. Figure 5 shows the proposed approach where

the object is freely moving in front of the laser scanner. The dual approach where the 3D scanner is moved relative to the object was also successfully tested as part of this work by holding the scanner in hand.

Figure 3: A 3D laser scanner on an unstable scaffolding structure; the working environment seriously compromises the accuracy of the range data.
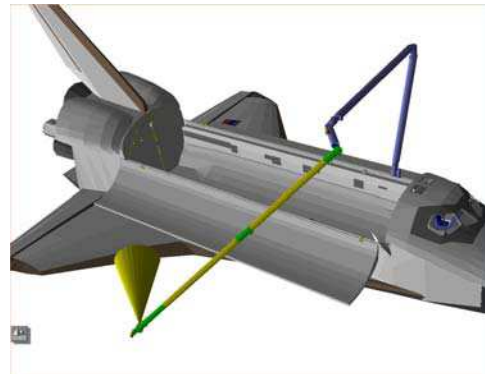
Figure 4: Application of 3D laser scanner for the inspection of the Space Shuttle fleet. The sensor is mounted on the tip of the boom extension. Because of the complexity of the arm-boom structure and many joints, constant oscillation of a few centimeters of amplitude and poor damping at the tip of the robot arm will be ever present.

Methods have been proposed to solve the problem of positioning the camera relative to the object without the use of external positioning devices. These methods are optimized for fast low-resolution object modeling; 3D accuracy and metrology are not their primary goal. The use of reference laser marks projected on the object and of a simplified surface model to reduce the calculation has been demonstrated in [1]. Good color texturing of a low-resolution 3D model and ease of use are the primary objectives. In [2] the authors are registering range data

acquired using laser profiles projected on the surface of the object, imaged by a CCD camera, to create a 3D map of the object surface. In [3], encoded patterns are used to freeze the motion of the object during the acquisition. Accuracy of the sensor system is better but still not sufficient for most metrology application because of the physical limits and resolution of the optical sensor head [4]. Each profile is considered a snapshot at instant *t*, blurring and motion during the integration of the light is not compensated.

The main constraint imposed to this development is accuracy. Real-time tracking and imagery is a must but the final optimization of the 3D model can be done remotely. The proposed method iteratively solves for 1) the relative pose of the camera/object (position and orientation), 2) the motion (speed), and 3) the change of motion (acceleration), for each rigel within a profile. At each iteration a better solution is obtained by: a) acquiring new 3D points, b) recursively re-calculating a better model of the object, and c) re-evaluating a better estimate of the previous and current relative camera-object motion.

Section 2 will present the laser scanner prototype used for this work and some practical constraints associated with the selection of the sensor and method. Section 3 will introduce the ICP based algorithm developed for object reconstruction and motion compensation. Experimental results are presented in Section 4.

Although this method was tested using a triangulation-based laser scanner, the algorithm presented in this paper can also be used with Time-of-Flight (TOF) laser scanners, and extended to profile and pattern projection systems [4].

2. The 3D Laser Scanner System – Practical Considerations

Figure 2 shows the 3D laser scanner prototype system used for this work. The control box contains all the electronics, laser and real-time tracking software and was constructed to survive abusive handling. Object modeling is implemented on a remote laptop or computer on the network; onboard data buffering and real-time software protects against latency and delays generated with Internet communication and non real-time operating systems such as Windows.

The advantages of this scanner system are described in [4] and [5]. The combination of excellent accuracy and large volume of measurement is a definite advantage compared to other methods. The use of Lissajous scanning patterns to obtain real-time tracking performances is shown in Figures 5 and 6 and explained in [6]. A Lissajous scanning pattern possesses many

interesting opto-mechanical properties and is the best compromise between scanning speed and accuracy, benefiting from the natural inertia of the scanning galvanometer-mirrors [6]. For each point on a profile a calibrated XYZ coordinate is obtained. In the case of Figures 5 and 6, 512 points are measured for each laser profile.

Figure 5: Hand-held 3D acquisition and real-time tracking using fast Lissajous scanning patterns. External constraints of rigidity are removed; no external positioning device is needed. This and the dual equivalent of holding the 3D camera were tested during this work. A priori object model is not needed; the model is reconstructed while tracking.
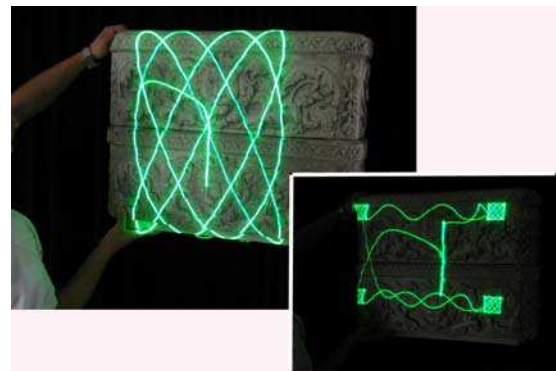

Figure 6: Variations of the scanning patterns, multiple Lissajous and combined Lissajous and raster/vector imaging.

Figure 6 combines Lissajous and raster scanning (one line) to acquire high-resolution accurate 3D images. Scanning patterns, dimensions, position and orientations are all user programmable. The more conventional raster type mode of imaging (line-by-line) produces a regular 3D grid that is needed by most software algorithms.

3. Algorithm

Object motion and Nyquist criteria

For the remaining of the paper, we assume that the input of the algorithm is a vector set of XYZ points from either a single Lissajous pattern, a raster line, a combined Lissajous-raster line, or any pattern. The length of a given XYZ profile is limited by the Nyquist criterion and by the relative motion of the object/sensor.

The acquisition rate and real-time operation are very important to characterize the maximum relative motion that can be measured. The motion is assumed to be relatively slow and its equivalent spectrum low in frequency content. Experience shows that mechanical oscillations in the 10 Hz to 100 Hz range are expected and that higher frequencies will be mostly damped because of the natural inertia (weight) of the 3D camera and/or object. From the Nyquist criteria and an acquisition rate of 10 kHz, a maximum of 100 to 1000 rigels/sec per range profile can be used for data registration without being hampered by aliasing.

Model creation

The introduction of Iterative Closest Point (ICP) registration algorithms or more generally the family of Iterative Corresponding Point methods [7-8-9-10-11] have greatly simplified the reconstruction of complex 3D models of objects acquired using 3D scanners. The Iterative Closest Point algorithms (ICP) have been developed mostly for solving the general problem of registration of static range images acquired from multiple partial views of a same object [8]. Many variations of these algorithms have been published but basically the objective is to find the best rigid transformation matrix that maps one set of range data to a reference set. This rigid transformation can then be used to stitch a new patch image to the reference surface. Several algorithms have been proposed to constrain convergence: minimizing the quadratic errors of the minimum distances between each point on the new patch and the reference surface (point-to-surface), between two surface patches (surface-to-surface), or between each point (point-to-point).

Mathematically, the objective of ICP algorithms is to find the rigid transformation matrix $\mathbf{M}_k$ that will align the range data set $\mathbf{x}_k$ in the scanner coordinate system with the model reference image data set $\mathbf{xm}_k$ where

$$\mathbf{xm}_k = \mathbf{M}_k \mathbf{x}_k \tag{1}$$

$$\mathbf{x}_k = \begin{bmatrix} x & y & z & 1 \end{bmatrix}^T \tag{2}$$

ICP algorithms generally assume that the data within the images are rigid, accurate, and most importantly, stable during the acquisition (still images). Thus, the 3D scanning process meets the requirement that the relative position between the scanner reference coordinate and the object under inspection is kept perfectly stable and distortion free.

From an initial set of sparse 3D points, the method presented here estimates a rough, partial, and potentially distorted model that provides a first approximation of the expected object. This model is also used to supervise the tracking of the object in a 3D space. New profiles are added to this initial set to recursively improve and refine the initial model. The final result is a high-resolution accurate representation of free-floating moving objects.

In [12] a simplified model estimation using the unity motion compensation matrix $\mathbf{D}_i = \mathbf{I}$ was presented. In this paper, the compensation matrix $\mathbf{D}_i$ is also estimated by calculating the speed and the motion acceleration.

Let us assume a subset $\mathbf{X}_k$ of N_k calibrated range data acquired by the range sensor. Each point $\mathbf{x}_i$ has an associated time tag t_i:

$$\mathbf{X}_k = \{\mathbf{x}_i; t_i\} \quad 0 \leq i < N_k \tag{3}$$

This subset corresponds to a single profile or a full pattern as illustrated in Figures 5 and 6. The time tag t_i is used to compensate for motion-induced distortions. Let us assume that $\hat{\mathbf{m}}_{k,i}$ is a point on an approximation of the real model $\mathbf{m}$. The problem of registration consists of finding the estimate $\hat{\mathbf{R}}_k$ of the rigid transformations $\mathbf{R}_k$ that minimizes the equation

$$\varepsilon_k = \sum_{i=0}^{N_k-1} \left\| \hat{\mathbf{m}}_{k,i} - \hat{\mathbf{R}}_k \hat{\mathbf{D}}_i \mathbf{x}_i \right\|^2 \tag{4}$$

The selection of the point $\hat{\mathbf{m}}$ depends on the ICP algorithm. $\hat{\mathbf{D}}_i$ is an estimate of the compensation matrix $\mathbf{D}_i$ that removes the residual distortions introduced by motion within the profile $\mathbf{X}_k$.

Let us also assume that we have a function $\Im$ that creates our estimate $\hat{\mathbf{m}}$ of the object from the K previous profiles or images:

$$\hat{\mathbf{m}}_{k,i} = \Im\left(\hat{\mathbf{R}}_k \hat{\mathbf{D}}_i \mathbf{x}_i\right) \quad \forall k,i \tag{5}$$

The function $\Im$ creates a mesh model from a set $\mathbf{X}_k$ of range points. The first model $\hat{\mathbf{m}}_0$ is obviously a very rough estimate, with the initial conditions $\mathbf{D}_i = \mathbf{I}$. The model creation procedure $\Im$ basically appends M new profiles to the previous model estimate $\hat{\mathbf{m}}_{k-M}$ that fill the gaps, expand its surface and refine the geometry of the new estimate $\hat{\mathbf{m}}_k$. The next step is to re-optimize the last model $\hat{\mathbf{m}}_k$ by iteratively re-evaluating the matrices $\hat{\mathbf{R}}_k$ and to better estimate $\hat{\mathbf{D}}_i$ and recreate a new model estimate $\hat{\mathbf{m}}$ that will minimize the total error

$$E = \sum_{k=0}^{K-1} \varepsilon_k \tag{6}$$

Optimization is fast and converges in a few iterations, especially if this optimization is implemented at the beginning of the optimization for a small number of subsets K, i.e.

$$\hat{\mathbf{R}}_k \approx \mathbf{R}_k \qquad \text{for } K \text{ small} \tag{7}$$

The practical implementation of this algorithm is presented in [12].

Speed and acceleration compensation

Speed and acceleration corrections are implemented by interpolating the estimates $\hat{\mathbf{D}}_i$ of the motion distortion matrix $\mathbf{D}_i$ for each measurement i using a function Ω and the rigel time tag t_i of Equation 3. Motion is interpolated from the relative trajectory of the object or scanner given by the matrices $\hat{\mathbf{R}}_k$

$$\hat{\mathbf{D}}_i = \Omega\left\langle \ldots, \hat{\mathbf{R}}_{k-1}, \hat{\mathbf{R}}_k, \hat{\mathbf{R}}_{k+1}, \ldots; t_i \right\rangle \tag{8}$$

Translations are easy to interpolate but rotations are a complete different matter especially when the rotation axis is not defined. The center of rotation can be any arbitrary point that can change with time. The problem is here simplified by assuming that *a translation is a rotation of infinite radius*. The objective is therefore to evaluate the best translation matrix $\mathbf{T}_{k^-}$ that will map $\hat{\mathbf{R}}_{k-1}$ to $\hat{\mathbf{R}}_k$ using rotations $\mathbf{Q}_{k^-}$ only. A linear interpolation of a rotation is then calculated using the

quaternion $\mathbf{q}_{k^-}$ of associated with the matrices $\mathbf{Q}_{k^-}$. The subscript k^- specifies that the previous data set k-1 is used to estimate the relative motion of the current data set k.

The interpolation of the profile k, using the previous profile position k-1 is therefore:

$$\mathbf{Q}_{k^-} = \mathbf{T}_{k^-} \cdot \hat{\mathbf{R}}_k \ ; \ \mathbf{Q}_{k-1} = \mathbf{T}_{k^-} \cdot \hat{\mathbf{R}}_{k-1} \tag{9}$$

$$\mathbf{Q}_{k^-} = \mathbf{T}_{k^-} \ \hat{\mathbf{R}}_{k-1}^{-1} \hat{\mathbf{R}}_k \mathbf{T}_{k^-}^{-1} \tag{10}$$

$$\mathbf{Q}_{k^-} = \begin{bmatrix} \mathbf{I} & \mathbf{Tr} \\ \mathbf{0} & 1 \end{bmatrix} \begin{bmatrix} \mathbf{M} & \mathbf{N} \\ \mathbf{0} & 1 \end{bmatrix} \begin{bmatrix} \mathbf{I} & -\mathbf{Tr} \\ \mathbf{0} & 1 \end{bmatrix} = \begin{bmatrix} \mathbf{Qm} & \mathbf{0} \\ \mathbf{0} & 1 \end{bmatrix} \tag{11}$$

Solving yields

$$\mathbf{Tr} = [\mathbf{M} - \mathbf{I}]^{-1} \cdot \mathbf{N} \tag{12}$$

$$\mathbf{T}_{k^-} = \begin{bmatrix} \mathbf{I} & \mathbf{Tr} \\ \mathbf{0} & 1 \end{bmatrix} \tag{13}$$

where $[\mathbf{M} - \mathbf{I}]^{-1}$ is the generalized inverse of a matrix. The profile $\mathbf{X}_k$ and matrix $\hat{\mathbf{R}}_{k-1}, \hat{\mathbf{R}}_k$ are first translated by $\mathbf{T}_{k^-}$ prior to compensation; interpolation between the rotation matrix $\mathbf{Q}_{k^-}$ and $\mathbf{Q}_{k-1}$ is done using a quaternion $\mathbf{q}_{k^-}$ and the time stamp t_i; and translated back to the profile original coordinate system.

Similarly, motion can also be estimated using the following profile k+1 rather than the previous set of data k-1. The matrix $\mathbf{T}_{k^+}$ is

$$\mathbf{Q}_{k^+} = \mathbf{T}_{k^+} \cdot \hat{\mathbf{R}}_k \ ; \ \mathbf{Q}_{k+1} = \mathbf{T}_{k^+} \cdot \hat{\mathbf{R}}_{k+1} \tag{14}$$

where k^+ specifies that the next profile k+1 is used. For a constant speed $\mathbf{Q}_{k^+} = \mathbf{Q}_{k^-}$; in practice $\mathbf{T}_{k^+} \neq \mathbf{T}_{k^-}$ and $\mathbf{Q}_{k^+} \neq \mathbf{Q}_{k^-}$ because of acceleration and the model estimate will be slightly different depending on how motion is estimated. In this paper, the acceleration estimate is simplified by assuming that the acceleration is a weighted change of rotation:

$$\mathbf{Q}_k = \alpha(t)\mathbf{Q}_{k^+} + (1 - \alpha(t))\mathbf{Q}_{k^-} \tag{15}$$

where $0 \leq \alpha(t) \leq 1$ is a weighting function with $\alpha(t_{k-1}) = 0$, $\alpha(t_k) = 0.5$, and $\alpha(t_{k+1}) = 1$.

It is possible to use more complex mathematical and more accurate methods such as smoothed interpolation using $\hat{\mathbf{R}}_{k-1}, \hat{\mathbf{R}}_k, \hat{\mathbf{R}}_{k+1}$, bi-cubic interpolations, or even a real physical model of the object. However because of the high sampling rate, the distortion created by acceleration is very small and this simplified linear weighted average produced excellent results.
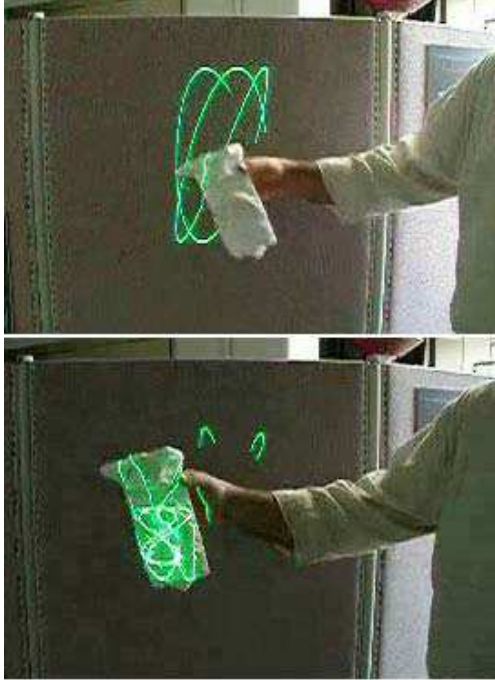
Figure 7: The laser scan detects an object that enters its field of view, automatically locks on it and tracks the object. At the same time, a smaller scanning pattern is projected on the object to acquire high-resolution 3D images.

After a few iterations, the final model of Equation 5 is a very close representation of the exact model

$$\hat{\mathbf{m}}_k = \mathbf{m} \quad ; \hat{\mathbf{R}}_k = \mathbf{R}_k \; ; \hat{\mathbf{D}}_i = \mathbf{D}_i \qquad (15)$$

4. Experimentation

Object modeling

In [12], the algorithm started with a low-resolution 128x128 raster image. Here the image is completely reconstructed from a single profile at the same time tracking is performed.

The model of the object is a priori not known; only its overall approximate dimensions are specified to instruct the scanner to lock on the object and to size the scanning patterns. As shown in Figure 7, the system first detects an object when it enters a specific volume (e.g. <2 m) within the field of view of the scanner. The algorithm then locks on the object's overall geometry and positions a large Lissajous pattern on its geometrical center-of-mass. A smaller scanning pattern is also simultaneously projected on the object to zoom on specific sections of the object to measure the very fine

Figure 8: Multi-resolution model of Figure 7 after k profiles.
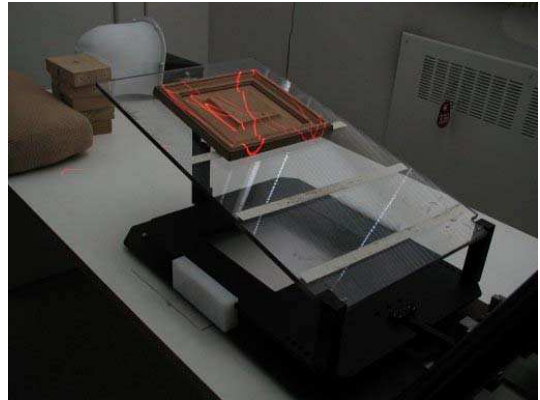

Figure 9: Experimental setup used to test the accuracy of the method and to simulate the expected experimental conditions of Figure 4. Oscillations are 3.5 cm of amplitude, 0.7 Hz, at a distance of 0.8 m from the camera.

details. This small high-resolution pattern is synchronized with the larger tracking pattern and finely swipes the object; a smaller Lissajous pattern is shown in Figure 7 while a raster profile was used in Figure 9. Figure 8 illustrates the results of the optimization; resolution and details are improving with the number of profiles and iterations. During tracking, the laser scan does not need to be perfectly centered on the object to obtain accurate pose estimates $\hat{\mathbf{R}}_k$.
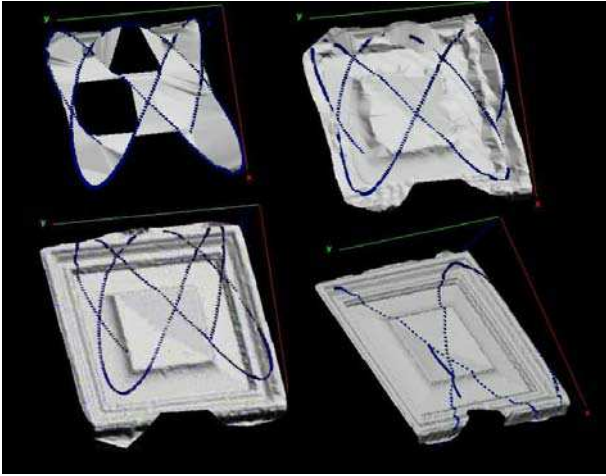
Figure 10: Multi-resolution model reconstruction of Figure 9. From the initial low-resolution and distorted model $\hat{\mathbf{m}}_0$ to the more refined version $\hat{\mathbf{m}}_k$. Very high-resolution imaging is obtained by zooming on specific sections of the object as shown in the bottom right image. The laser profile pattern is superimposed on the reconstructed model.

Accuracy: speed and acceleration compensation

The experimental setup of Figure 9 was used to test the accuracy of the proposed method. A small pyramidal object is mounted on an oscillating table at a nominal distance of 0.8 m from the camera. The motion of the table is a-priori not known; speed and amplitude of the motion were set to the maximum values possible with this mechanical setup (3 cm @ 0.7 Hz). This experimental setup was used to test worst-case conditions that can be expected in applications similar to Figure 4. As opposed to flat surfaces such as the shuttle tiles that will test only the Z accuracy, the pyramid of Figure 9 also allows testing of all X,Y,Z measurements.

Figure 10 shows the model reconstruction process. The algorithm starts with a single Lissajous profile and the model is refined at the same time that profiles are added. Because of the non-deterministic and non real-time nature of ICP algorithms, this operation is performed in parallel; the algorithm only supervises the tracking process of Figure 7.

Figure 11 shows the image created by the raw range data at different iteration steps. The distortion introduced by the motion of the table is obvious in the original non-compensated data. At each iteration, the model is dramatically improved. The residual error for the model of Figure 11 is 200 um without speed compensation ($\mathbf{D}_i = \mathbf{I}$). With speed and acceleration
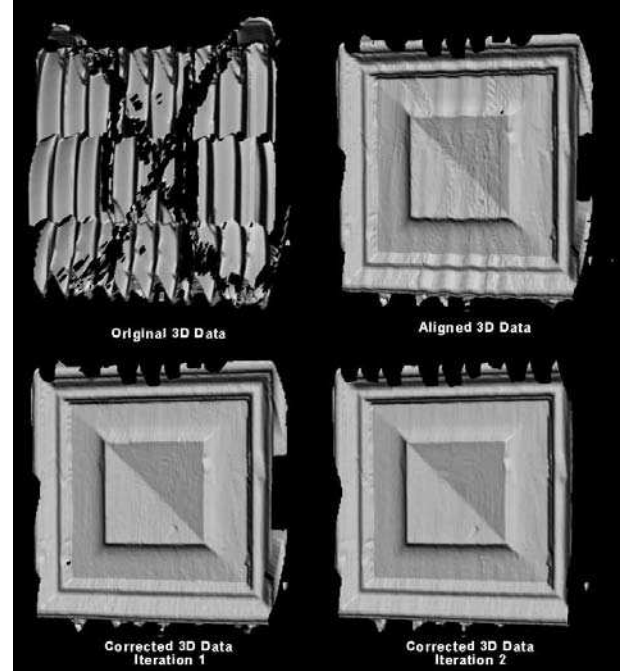

Figure 11: Results of the recursive optimization algorithm: top-left) original distorted raw profiles; top-right) initial alignment, bottom-left) after one iteration; bottom-right) after two iterations. After four iterations, the differences between dynamic imaging (motion) and static imaging (no motion) are insignificant.

compensation, this residual error is further reduced to 175 um and 140 um respectively. A comparison between this model and the same object acquired in static mode (no motion) shows no significant difference; the residual RMS errors are very similar and in fact slightly better.

The most important key factor that affects the quality of the results is calibration of the range data and the compensation of its internal dynamic properties associated with the time stamp t_i. Most scanners produce range data in the form $\mathbf{x} = \begin{bmatrix} x & y & z & 1 \end{bmatrix}^T$, which is only an approximation of the true form $\mathbf{x} = \begin{bmatrix} x(t) & y(t) & z(t) & 1 \end{bmatrix}^T$. This approximation is valid only when the scanner is used in static mode. Dynamic calibration implies that the range data must be converted in the form of Equation 3, the time stamp t_i becomes and independent variable, uncorrelated with respect to *x*, *y*, and *z*.

5. Conclusion

This paper has presented a recursive optimisation method that, when combined with sparse range data, can produce high quality, high-resolution 3D range images. The algorithm first creates a very rough and distorted model of a moving object and recursively optimises the model using newly acquired range information and from a better estimate of the object motion. Speed and acceleration compensation for each XYZ point in the image provides a very accurate model of the real object.

The method was tested with a single spot laser scanner. Real-time tracking of free moving objects while creating high-resolution images was demonstrated providing a truly high-accuracy hand-held 3D laser scanning system. The accuracy obtained of a moving object is comparable to static imaging (when object/camera is not moving).

The main objective and use of this work is to create high resolution and accurate 3D models of objects without requiring complex and expensive mechanical infrastructures normally associated with laser scanner systems. Examples of situations where the application cannot benefit from a mechanically stable environment and hard to reach objects are numerous such as for example when using scaffoldings to scan detailed façades of historical buildings, or when the sensor is mounted on robotic arms or on moving vehicles.

6. References

[1] V.Popescu, E.Sacks, G.Bahmutov, "The ModelCamera: a Hand-Held Device for Interactive Modeling", Proc. 3DIM 2003, 285-292, 2003.

[2] P. Hébert, "A self-referenced hand-held range sensor", Proc. 3DIM 2001, 5-12, 2001.

[3] T.P.Koninckx, A.Griesser, L.Van Gool, "Real-time Range Scanning of Deformable Surfaces by Adaptively Coded Structured Light", Proc. 3DIM 2003, 293-300, 2003.

[4] F.Blais, "Review of 20 Years of Range Sensor Development", Journal of Electronic Imaging, 13(1), 231-240, Jan. 2004.

[5] F.Blais, J.-A.Beraldin, L.Cournoyer, I.Christie, K.Mason, S.McCarthy, C.Goodall, "Integration of a tracking laser range camera with the photogrammetry based space vision system", Proc. Acquisition, Tracking and Pointing XIV, SPIE 4025, 219-228, 2000.

[6] F.Blais,J.-A.Beraldin,S.F.El-Hakim, L.Cournoyer, "Real-time geometrical tracking and pose estimation using laser triangulation and photogrammetry", 3DIM 2001,205-212, 2001.

[7] S. Rusinkiewicz, M.Levoy, "Efficient variant of the ICP algorithm", Proc. 3DIM 2001, 145-152, 2001.

[8] P.J.Besl, N.D.McKay, "A method of registration of 3D shapes". IEEE Transactions on Pattern Analysis and Machine Intelligence, 14(2), 239-256, Feb. 1992.

[9] R. Bergevin, M.Soucy, H.Gagnon, D.Laurendeau, "Towards a general multi-view registration technique", Trans. PAMI, 18(5), 1996.

[10] G.Godin, D.Laurendeau, R.Bergevin, "A method for the registration of attributed range images", Proc. 3DIM 2001, 179-186, 2001.

[11] Y.Chen, G. Medioni, "Object modeling by registration of multiple range images", Image and Vision Computing, 10(3), 145-155, April 1992.

[12] F. Blais, M.Picard, G.Godin, "Recursive Model Optimization Using ICP and Free Moving 3D Data Acquisition", Proc. 3DIM 2003, 251-258, 2003.